Th. 162

ORNL/TM-6318

178
6-16-78

A Preliminary Investigation of Trapped Particle Instabilities in EBT

D. B. Batchelor
C. L. Hedrick

OAK RIDGE NATIONAL LABORATORY
OPERATED BY UNION CARBIDE CORPORATION · FOR THE DEPARTMENT OF ENERGY

DISCLAIMER

Printed in the United States of America. Available from
National Technical Information Service
U.S. Department of Commerce
5285 Port Royal Road, Springfield, Virginia 22161
Price: Printed Copy ~~$5.25~~ 4.50; Microfiche $3.00

ORNL/TM-6318
Dist. Category UC-20g

Contract No. W-7405-eng-26

FUSION ENERGY DIVISION

A PRELIMINARY INVESTIGATION OF TRAPPED PARTICLE INSTABILITIES IN EBT

D. B. Batchelor
C. L. Hedrick

Date Published - May 1978

NOTICE This document contains information of a preliminary nature. It is subject to revision or correction and therefore does not represent a final report.

Prepared by the
OAK RIDGE NATIONAL LABORATORY
Oak Ridge, Tennessee 37830
operated by
UNION CARBIDE CORPORATION
for the
DEPARTMENT OF ENERGY

THIS PAGE

WAS INTENTIONALLY

LEFT BLANK

CONTENTS

THIS PAGE

WAS INTENTIONALLY

LEFT BLANK

ABSTRACT. An investigation is presented of the role which trapped particles might play in the drift wave stability of ELMO Bumpy Torus (EBT). The model adopted consists of a bounce-averaged drift kinetic equation with a Krook collision operator. Care has been taken to model, at least in an elementary way, the features which distinguish the physics of EBT from that of tokamaks, namely the large magnitude and velocity space dependence of the poloidal drift frequency Ω, the relatively small collisionality ν/Ω, the enhancement of ν_{eff} for passing particles, and the closed nature of the field lines. Instabilities are found which have a somewhat dissipative character, however the precessional drift is found to be a significant stabilizing influence. In most cases, the modes are completely stabilized when $\omega_*/\ell\Omega \lesssim 1$ for normal gradients. For reversed gradients ($\omega_*/\ell\Omega < 0$), stability is greatly enhanced.

1. INTRODUCTION

Because of the apparent importance of the various trapped particle instabilities with regard to the scaling of tokamaks to reactor size devices, and because of the relatively large population of trapped particles in ELMO Bumpy Torus (EBT) devices, we have conducted a preliminary investigation of the role which trapped particles might play in the drift wave stability of EBT. Since the field line geometry, particle orbits, and frequency relationships in EBT are so entirely different from those in tokamaks, we feel that the advanced theory of trapped particle modes developed for tokamaks is not directly applicable to EBT. Instead we have adopted the very simplest model which contains the basic EBT physics. The model consists of a bounce-averaged drift kinetic equation with an energy dependent Krook collision operator. This is much in the spirit of the early work on trapped particle modes in tokamaks where the realism was absent (radial mode structure, finite Larmor radius effects, complicated collision operators, etc.), but the basic instability mechanism was present [1,2].

The most striking dissimilarity between EBT and a tokamak is the method of single particle confinement. In EBT the vertical drift of the particles due to toroidicity is averaged out by a rapid poloidal drift, Ω, associated with mirror curvature, magnetic field gradients, and radial ambipolar electric field, $\Omega = \Omega_{\text{curvature}} + \Omega_{\nabla B} + \Omega_{E\times B}$; whereas in tokamaks, particles move poloidally by following the rotational transform of the field lines. The shape of the trapped particle orbits is entirely different in the two devices. In EBT the poloidal drift frequency, Ω, for trapped particles is small compared to the bounce frequency ($\Omega \ll \omega_b$),

so that a single bounce covers a very small poloidal angle. However, Ω can be comparable to or exceed the minimum diamagnetic drift frequency, ω_{*min}, and the electron collision frequency, ν_e. In tokamaks, trapped particle orbits are predominantly thin bananas extending along a field line and covering a considerable poloidal angle. On a much longer time scale, $\omega_D \ll \omega_*$, the bananas in tokamaks drift in the toroidal direction due to magnetic curvature. For comparison then, on the ω_*^{-1} time scale, we can picture tokamak trapped particles to be confined to a thin tube about a field line until a collision occurs; whereas EBT trapped particles move away from field lines on a drift surface on this time scale.

In addition, there is considerable spatial disperison of particle orbits in EBT. Since the precessional frequency and the inward shift of particle orbits depend on energy and pitch angle, particles which are close together at a given time will spread apart both radially and poloidally on a time scale $\tau \sim \Omega^{-1}$. This short particle correlation time makes it difficult for the collective modes to occur with frequencies $\omega \sim \omega_D = \ell\Omega$. Of course, it also makes calculation of such modes extremely difficult.

Absence of rotational transform also has an important effect on passing particles. In a tokamak the passing particles respond only adiabatically to an electrostatic wave except possibly on a mode rational surface. In EBT the field lines are closed and passing particles may see a nonvanishing perturbed average potential. In this case passing particles will also respond nonadiabatically. Because they must average over regions of positive and negative magnetic curvature, the precessional

drift speed is slower for passing particles than it is for trapped particles. Typically, $\Omega_{passing} \sim 0.1\ \Omega_{trapped}$.

Finally, the partitioning of velocity space among trapped and passing particles is reversed from tokamaks to EBT. In EBT, it is the passing fraction which is small (typically 25-30%). The effective collision frequency for passing particles is therefore much larger than for the trapped particles, $\nu_{j\ passing} \sim \nu_{j\ trapped}/(1 - f_T^2)$, where f_T is the fraction of trapped particles. In several respects the role of passing and trapped particles is reversed from tokamaks to EBT.

In Section 2 estimates of the various quantities which enter the stability theory are discussed in detail. Typical values are given for the current device, EBT-I, and projected values to the ELMO Bumpy Torus Reactor (EBTR) reference design. Models for the drift orbits and collision operator are described and an appropriate bounce-averaged drift kinetic equation is presented. In Section 3 calculations are presented for modes in which the passing particles are assumed to behave adiabatically. An unstable mode is found which behaves in some respects like a dissipative trapped particle mode. However, the magnetic precessional drift is shown to be a significant stabilizing influence. In Section 4 calculations are presented for pure flute modes in which the passing particles can have a nonadiabatic response. Again a dissipative type mode is found. In Section 5 the results are summarized and the possible effects of the instabilities are discussed. Areas for improvement of the model are mentioned.

2. FREQUENCY ORDERINGS AND THE DRIFT KINETIC MODEL

Since little has previously been published concerning the kinetic theory of low-frequency instabilities in EBT, it is perhaps worthwhile to go into detail about the ordering of the various time scales in EBT. Table I contains a list of typical parameters for EBT-I and for the EBTR reference design [3,4]. Because of the presence of the high beta electron annulus in EBT devices, there exists radial structure in the equilibrium profiles having scale length much different from the minor radius a. The details of the equilibrium profiles are important, and simple frequency estimates based on major and minor radius as characteristic scale lengths may be misleading. Figure 1a shows a typical profile of B/B_0 at the midplane. In the core region, B decreases gradually, which is characteristic of the vacuum mirror fields. In the annulus region, a magnetic well exists with large values of ∇B. At the outer portion of the annulus, ∇B reverses sign.

It should be emphasized that wide variations in density scale length are also expected across the EBT profile. One-dimensional (1-D) neoclassical transport calculations show very flat density and temperature profiles in the core region with steep gradients on the outside [5]. Enhanced neoclassical confinement in the annulus region, due to large precession frequency Ω (not as yet included in the 1-D transport model), should increase this character of the profiles. In addition, the requirements of MHD stability dictate a reasonably flat pressure profile in the core region. These effects suggest a density profile of the form shown in Fig. 1a. No detailed measurements of either magnetic field or density profiles are available at this time.

We will be concerned with drift waves having frequency $\omega \sim \omega_{*e} = k_\perp T_e/m_e\omega_{ce}L_n$, where $k_\perp = \ell/r$, ℓ is the poloidal mode number, and $L_n^{-1} = d\,(\ell n\ n)/dr$ is the density gradient scale length. For a Gaussian density profile $n(r) = n_0 \exp(-r^2/a^2)$, we have $L_n = -a^2/2r$ and $\omega_* = 2\ell\, T_e/m_e\omega_{ce}a^2$. Using this estimate, typical values for the minimum ($\ell = 1$) and maximum ($\ell = a/\rho_i$) of ω_* are shown in Table II for EBT-I and EBTR. These numbers are illustrative, however, if the density profile is of the form shown in Fig. 1a; ω_* will be significantly smaller in the core region and significantly larger in the outer portion of the annulus region. The resultant ω_* profile is shown in Fig. 1b.

A quantity of fundamental importance for both transport and drift wave stability in EBT is the bounce- or transit-averaged poloidal drift (or precessional) frequency Ω

$$\Omega = \Omega_{\nabla B} + \Omega_{E\times B} \tag{1}$$

where

$$\Omega_{\nabla Bj} = \left\langle \frac{1}{r}\frac{v^2}{\omega_{cj}}\left[\left(\frac{v_\parallel}{v}\right)^2 \frac{d\hat{b}}{d\ell} + \frac{1}{2}\left(\frac{v_\perp}{v}\right)^2 \hat{n}\times\nabla\ \ell n\ B\right]\right\rangle_{\text{bounce average}}$$

$$\Omega_{E\times B} = \left\langle \frac{c}{r}\frac{\underset{\sim}{E}\times\underset{\sim}{B}}{B^2}\right\rangle_{\text{bounce average}} \tag{2}$$

$$\hat{n} = \frac{\underset{\sim}{B}}{B}$$

$$\omega_{cj} = e_j B/m_j c$$

The precessional frequency is strongly dependent on particle energy and pitch angle as well as on the radial location of the drift surface. Sizable electric fields are observed in EBT ($e\phi \sim T_i$) so that the E × B component of Ω is quite important on neoclassical transport time scales [6]. However, the bounce average of E_r/B is independent of pitch angle, and $\Omega_{E\times B}$ is nearly equal for electrons and ions. Therefore, $\Omega_{E\times B}$ will be neglected in the present calculations.

For particles near the axis in the low beta region, $\Omega_{\nabla B}$ can be found analytically in terms of elliptic integrals if a model bumpy-cylinder magnetic field configuration is assumed [7]. In order to treat the high beta annulus region as well as the low beta core, we have used an analytic fit to numerically computed orbits. The precessional drift frequency $\Omega_{\nabla B}$ was calculated as a function of c and ζ_m using a specific finite-beta equilibrium magnetic field configuration obtained from the Oak Ridge 2-D equilibrium code [8], where

$$c^2 = \frac{m_i v^2}{2T_i}$$

$$\zeta_m = \frac{v_{\parallel m}}{v} = \text{cosine of pitch angle at midplane}$$

$$v = \text{particle velocity} \tag{3}$$

$$v_{\parallel m} = v_{\parallel} \text{ evaluated at a minor midplane}$$

It is most convenient to express $\Omega(c,\zeta_m)$ in the form

$$\Omega(c,\zeta_m) = \Omega_0 \Omega'(c,\zeta_m)$$

where

$$\Omega_0 = \frac{2\pi^2 T_j}{m_j \omega_{cj} L_s^2} \tag{4}$$

where L_s is the length of a single mirror segment and Ω' is a dimensionless, velocity-space form factor in which $\Omega'(c,\zeta_m)/c^2$ depends on ζ_m. The model used here for the orbits is substantially the same as that used by Spong in the calculation of neoclassical transport coefficients [9].

Figure 2 shows Ω'/c^2 as a function of ζ_m for points in the low beta region and in the high beta, reversed ∇B region. The form of these curves can be understood qualitatively as follows. Deeply trapped particles ($\zeta_m \ll 1$) see magnetic radius of curvature R_c, and ∇B of one sign only and therefore have large $|\Omega'|$. Particles near the trapped/passing boundary ($\zeta_m = 0.7$ in the low beta region) see alternating signs of R_c and ∇B hence have small or even positive Ω'. For strongly passing particles ($\zeta_m \cong 1$), the curvature drift dominates ∇B drift, and Ω' is negative but small. In the high beta region, Ω' is large and positive for $\zeta_m \ll 1$ due to the strong positive magnetic field gradient.

A good analytic fit to the curves in Fig. 2 is obtained in the low beta region from

$$\frac{\Omega'}{c^2} = \begin{cases} \alpha_0^T - \alpha_1^T \zeta_m^2 \ , \ \alpha_0^T = 1.0 \ , \ \alpha_1^T = 2.22 \quad \text{for} \quad 0 \leq \zeta_m \leq 0.7 \\ \alpha_0^P - \alpha_1^P (1 - \zeta_m)^2 \ , \ \alpha_0^P = 0.119 \ , \ \alpha_1^P = 2.174 \quad \text{for} \quad 0.7 \leq \zeta_m \leq 1 \end{cases} \tag{5}$$

and in the high beta region from

$$\frac{\Omega'}{c^2} = \alpha_0 + \alpha_1 \zeta_m^2 \ , \ \alpha_0 = -5.0 \ , \ \alpha_1 = 6.37 \ , \quad \text{for} \quad 0 \leqslant \zeta_m < 1 \tag{6}$$

An effective thermal precessional frequency $\langle\Omega\rangle$ can now be defined by averaging over an isotropic Maxwellian distribution

$$\langle\Omega\rangle = \int d^3v \ \Omega(c,\zeta) F_m(v) = \Omega_0 \langle\Omega'\rangle \tag{7}$$

Using the forms given in Eqs (5) and (6) for Ω', we obtain $\langle\Omega'\rangle = -0.717$ in the low beta region and $\langle\Omega'\rangle = 2.95$ in the high beta region. Typical values of $\langle\Omega\rangle$ in the low and high beta regions are given in Table II for EBT-I and EBTR. It can seen that $\langle\Omega\rangle$ is of the same order as ω_{*min}. Comparing the particle drift frequency, which appears in the stability theory ($\omega_D = \ell\Omega$) with ω_* given above, we find that

$$\frac{\omega_*}{\langle\omega_D\rangle} = \frac{\omega_*}{\ell\Omega_0\langle\Omega'\rangle} = \frac{L_s^2}{\pi^2 a^2 \langle\Omega'\rangle}$$

In the low beta region $\omega_*/\omega_D \cong 1$ for EBT-I, and $\omega_*/\omega_D \cong 6$ for EBTR. Because of the magnetic well, ω_D varies greatly over the radial extent of the plasma. A typical profile for $\langle\omega_D\rangle$ is shown in Fig. 1b.

It is also of interest to consider separately the averages of Ω over the trapped and passing particle populations. Using Eq. (7), we find that in the low beta region $\langle\Omega'\rangle_{trapped} = 0.99$ and $\langle\Omega'\rangle_{passing} = 0.08$. Therefore, the average precession frequency for trapped particles is an order of magnitude larger than that for passing particles.

Since the trapped particles in an EBT device are confined to a single short mirror sector, the bounce frequencies of both species of particles $\omega_{bj} \cong v_j/L_s$ are quite large. Typical values for EBT-I and EBTR can be found in Table II. For electrons, both ω_b and the transit frequency of passing particles $\omega_{Tj} \cong v_j/R_T$ are much larger than wave frequencies of interest. Hence the use of a bounce- or transit-averaged drift kinetic equation is justified for electrons. For ions, the bounce and transit frequencies are not much larger than ω_{*min}, so the use of a bounce-averaged drift kinetic equation is strictly valid only for comparatively low frequency modes.

The Spitzer collision frequencies

$$\nu_j = \frac{4\pi n_j e^4 \ell n \Lambda}{\sqrt{m_j}\,(2T_j)^{3/2}} \tag{8}$$

are given in Table II for EBT-I and EBTR. It can be seen that $\nu_j \ll \omega_{bj}$, ω_* for both species. In tokamak parlance, EBT is deep into the banana regime. Since most of velocity space in EBT is trapped, the enhancement of the effective collison frequency over the Spitzer value is modest for trapped particles

$$\nu_{jT} = \frac{\nu_j}{f_T^2} \cong 2\nu_j \tag{9}$$

if $f_T \cong 0.7$ as is appropriate for a 2:1 mirror ratio. On the other hand, the passing particles occupy only a narrow wedge in velocity space and have a much larger effective collision frequency

$$\nu_{jP} = \frac{\nu_j}{(1 - f_T)^2} \cong 10\nu_j \tag{10}$$

In this work we have used an energy dependent Krook collision operator,

$$C_j h_j = -\nu_{j\ \mathrm{eff}}(E) h_j = \begin{cases} -\nu_{jT}\left(\frac{E}{T_j}\right)^{-3/2} h_j \ , \text{ trapped particles} \\ -\nu_{jP}\left(\frac{E}{T_j}\right)^{-3/2} h_j \ , \text{ passing particles} \end{cases} \tag{11}$$

where h_j is the nonadiabatic part of the perturbed distribution function, and the effective trapped and passing collision frequencies ν_{jT}, ν_{jP} are defined in Eqs (9) and (10).

The appropriate coordinates for describing a bumpy torus are ψ — a radial-like field line label, χ — a poloidal angle-like field line label, and ζ — the toroidal angle. The present work will be carried out in the axisymmetric bumpy cylinder limit (Fig. 3), where ψ is the magnetic (toroidal) flux, θ is the azimuthal angle, and z is measured along the length of the cylinder. The total length of the cylinder is $L_T = 2\pi R_T$, where R_T is the major radius. The length of a single segment, L_s (i.e., distance between successive mirror throats) is just $L_s = L_T/N$, where N is the number of segments.

In terms of the coordinates ψ,θ,z, we assume the equilibrium distribution function to be an isotropic Maxwellian on each ψ surface

$$F^0(\underset{\sim}{x},E,\mu) = F_m(E,\psi) = n_0(\psi)\left[\frac{m_j}{2\pi T_j(\psi)}\right]^{3/2} \exp\left[-\frac{m_j E}{2T_j(\psi)}\right] \tag{12}$$

The perturbed distribution function δf is divided into an adiabatic response and a nonadiabatic response δh where,

$$\delta f(\underset{\sim}{x},E,\mu) = \frac{e_j}{m_j}\,\delta\phi(\underset{\sim}{x})F_{mj}(E,\psi) + \delta h(\underset{\sim}{x},E,\mu) \tag{13}$$

and δh is constant along a field line to lowest order in ω/ω_b. Fourier analyzing in t and θ all perturbed quantities can be written in the form

$$\delta\phi(\underset{\sim}{x}) = \phi(s,\psi)e^{i(\ell\theta-\omega t)} \tag{14}$$

The bounce-averaged drift kinetic equation h_j can now be expressed in the form [10]

$$(\omega - \omega_{Dj})h_j - i\overline{C(h_j)} = \frac{e_j}{T_j}\,[\omega - \omega^*_{Tj}(E)]\bar{\phi}\,F_{mj}(E,\psi) \tag{15}$$

where

$\omega_{Dj} = \ell\Omega(E,\mu)$ = bounce-averaged particle drift frequency

$\overline{C(h_j)}$ = bounce-averaged collision operator

$$\omega^*_{Tj}(E) = \omega_{*j}\left[1 + \eta_j\left(\frac{m_jE}{T_j} - \frac{3}{2}\right)\right] = \text{total diamagnetic frequency}$$

$$\omega_{*j} = \frac{\ell T_j}{m_j\omega_{cj}}\,\frac{1}{r}\,\frac{B}{n_0}\,\frac{dn_0}{d\psi} - \text{diamagnetic frequency}$$

$$\eta_j = d\ \ell n\ T_j/d\ \ell n\ n_0$$

$$\bar{\phi}(E,\mu,\psi) = \frac{\oint \frac{ds}{v_{\parallel}(E,\mu,s)}\,\phi(s)}{\oint \frac{ds}{v_{\parallel}(E,\mu,s)}} = \text{bounce-averaged perturbed potential}$$

With the Krook-type collision operator, Eq. (15) is simply an algebraic equation for h_j, which is solved to give

$$h_j(\psi,E,\mu) = \frac{e_j}{T_j}\,\frac{\omega - \omega_{Tj}^*}{\omega - \omega_{Dj} + i\nu_{eff}}\,\bar{\phi}\,F_m(E) \tag{16}$$

The stability of electrostatic perturbations in the quasi-neutral approximation is described by the equation

$$0 = \sum_j e_j \delta n_j = \sum_j -\frac{e_j^2}{T_j}\left[\phi - \int d^3v\,\frac{\omega - \omega_{Tj}^*}{\omega - \omega_{Dj} + i\nu_{eff}}\,\bar{\phi}(E,\mu)F_m(E)\right] \tag{17}$$

When written in terms of the velocity space variables c and ζ_m [see Eq. (3)], the velocity space integral becomes

$$\int d^3v[\cdot] \to 4\pi\left(\frac{m_j}{2\pi}\right)^{-3/2}\int_0^{\infty} dc\; c^2 \int \frac{d\zeta_m}{\sqrt{1 - \frac{B_{min}}{B(s)}}}\,\frac{\frac{B(s)}{B_{min}}\,\zeta_m}{\sqrt{1 - \frac{B(s)}{B_{min}}(1 - \zeta_m^2)}}\,[\cdot] \tag{18}$$

and the dispersion relation can be written in the form

$$\sum_j \frac{\omega_j^2}{T_j}\left\{\phi(\psi,s) - \frac{4}{\sqrt{\pi}}\int_0^{\infty} dc\; c^2 e^{-c^2} \int \frac{d\zeta_m}{\sqrt{1 - \frac{B_{min}}{B(s)}}}\,\frac{\frac{B(s)}{B_{min}}\,\zeta_m\bar{\phi}(\zeta_m)}{\sqrt{1 - \frac{B(s)}{B_{min}}(1 - \zeta_m^2)}} \times \frac{[\omega - \omega_{Tj}^*(c)]}{\omega - \omega_{Dj}(c,\zeta_m) + i\nu_{j\ eff}(c)}\right\} = 0 \tag{19}$$

We now consider the nature of the mode structure along the magnetic field lines. The potential $\phi(s)$ must be periodic in making a complete circuit of the torus and can be expanded in a Fourier series in arc length along a field line s

$$\phi(s) = \sum_{n=-\infty}^{\infty} \alpha_n e^{2\pi n i s/\Lambda} = \sum_{n=-\infty}^{\infty} \alpha_n \exp\left(2\pi i \frac{n}{N}\frac{s}{\Lambda_s}\right) \tag{20}$$

where

$$\Lambda = \oint ds = \oint dz \sqrt{1 + \frac{B_r^2}{B_z^2}} = \text{total length of field line}$$

$$\Lambda_s = \Lambda/n = \text{the length of a field line within one sector}$$

For passing particles the transit average of the potential vanishes except for the contribution from the constant part of $\phi(s)$ (i.e., α_0). In general the dispersion relation can be written

$$\sum_j \frac{1}{T_j}\left[\phi(s) - \int_{\text{trapped}} d^3v \frac{\omega - \omega_{Tj}^*}{\omega - \omega_{Dj} + i\nu_{j\ \text{eff}}} F_m \bar{\phi}(\zeta_m) - \alpha_0 \int_{\text{passing}} d^3v \frac{\omega - \omega_{Tj}^*}{\omega - \omega_{Dj} + i\nu_{j\ \text{eff}}} F_m\right] = 0 \tag{21}$$

Now in order that the perturbations are not strongly Landau damped by the ions, it is necessary that the parallel phase velocity be much larger than the ion thermal speed, $\omega/k_\parallel \gg v_i$. If ω is estimated by ω_{*e}, the condition becomes

$$\lambda_{\parallel} \gg \frac{\pi}{\ell} \frac{T_e}{T_i} \frac{a}{\rho_i} a$$

For both EBT-I and EBTR, the factor $aT_e/\rho_i T_i$ is quite large ($\sim$100). Now $\pi a \cong L_s$, and it is clear that for the lower frequency modes ($\ell \sim 1$) $\lambda_{\parallel}$ must be longer than the toroidal length Λ. As $\phi(z)$ must be periodic, the modes must be essentially flute-like ($\alpha_n \cong 0$ for $n \neq 0$). Even for the highest frequency modes ($\ell \sim a/\rho_i$), the parallel wavelength must be long ($\lambda_{\parallel} \gg \pi a \sim L_s$) so that the $\phi(z)$ varies only slightly within a single mirror sector (i.e., $\alpha_n = 0$ for $n \gtrsim N$). Therefore $\bar{\phi}$ has a very weak dependence on ζ_m and can be taken outside of the velocity space integral over trapped particles [$\bar{\phi}(\zeta_m) \cong \phi(s)$]. Under these circumstances, the dispersion relation can be written

$$\sum_j \frac{1}{T_j} \left\{ \phi(s) \left[1 - \int_{\text{trapped}} d^3v \frac{\omega - \omega_{Tj}^*}{\omega - \omega_{bj} + i\nu_{j\ \text{eff}}} F_m(E) \right] - \alpha_0 \int_{\text{passing}} d^3v \frac{\omega - \omega_{Tj}^*}{\omega - \omega_{Dj} + \nu_{j\ \text{eff}}} F_m(E) \right\} = 0 \qquad (22)$$

It should be mentioned that the ansatz that $\phi(s)$ does not vary on the length scale Λ_0 (i.e., $\alpha_n = 0$ for $n \gtrsim N$) is not completely self-consistent. Because the limits of the ζ_m integration contain $B(s)$ [see Eq. (18)], the pitch angle dependence of ω_D induces a variation along the field line in the nonadiabatic response even if $\bar{\phi}$ is independent of ζ_m. This is manifested, for example, in Eq. (22) by the velocity space integrals, which are functions of s, but are required to balance a constant unity. In the present work we do not attempt to solve for the mode

structure along the field line. Instead we neglect the additional variation with s and resort to what amounts to a slab approximation; that is, the ζ_m integral is evaluated at the midplane of each mirror sector, $B(s) = B_{min}$,

$$\frac{\int^{1} d\zeta_m}{\sqrt{1 - \frac{B(s)}{B_{min}}}} \frac{\frac{B(s)}{B_{min}} \zeta_m}{\sqrt{1 - \frac{B(s)}{B_{min}} (1 - \zeta^2_m)}} [\cdot] \rightarrow \int_0^1 d\zeta_m [\cdot] \tag{23}$$

Here, without solving for the mode structures, we consider the results of making two alternative assumptions on the potential: (1) the case of pure flute modes ($\alpha_n = \delta_{n0}$) or (2) the case in which the average potential along a field line α_0 vanishes and passing particles have only an adiabatic response. The later case corresponds to the situation in tokamaks for which the constant part of the perturbed potential must vanish except exactly on a mode rational surface. This points out an interesting difference between drift waves in EBT and in tokamaks. Since the field lines in EBT are closed, it is possible for different field lines on the same ψ surface to have different net potential, $\alpha_0 \neq 0$. As a result, the passing particles in EBT can have a nonadiabatic response to low frequency drift waves [last term in Eq. (22)].

3. MODES IN WHICH PASSING PARTICLES RESPOND ADIABATICALLY

We consider first the case in which the average along a field line of the perturbed potential is assumed to vanish. In this circumstance, the passing particles have no nonadiabatic response, and the stability

properties are described by Eq. (22) with $\alpha_0 = 0$. Even with all the simplifications made so far, Eq. (22) is still quite complicated, and solutions must be obtained numerically. Much insight can be obtained, however, by replacing integrals over velocity dependent frequencies $[\omega_j^*(E),\ \omega_{Dj}(E,\zeta),\ \nu_j(E)]$ by characteristic values. The dispersion relation thus obtained has the form

$$\frac{1}{T_e} + \frac{1}{T_i} = f_T \left(\frac{1}{T_e} \frac{\omega - \omega_{*e}}{\omega - \omega_{DeT} + i\nu_{eT}} + \frac{1}{T_i} \frac{\omega - \omega_{*i}}{\omega - \omega_{DiT} + i\nu_{iT}} \right) \tag{24}$$

where ω_{DjT}, ν_{jT} are effective frequencies suitably averaged over the trapped region of velocity space, and ω_{*j} is the basic diamagnetic frequency defined after Eq. (15).

Equation (24) is quadratic in ω and can be solved immediately to yield an expression for the growth rate. If one assumes $T_e = T_i$ and neglects ν_{iT} in comparison with ν_{eT}, a simple expression for ω is obtained

$$\omega = \frac{1}{4(1 - f_T)} \left(-\nu_{eT}(2 - f_T)i \pm \left\{ 16(1 - f_T) \left[(\omega_{De}^2 - \omega_{De}\omega_{*e}) - i\nu_{eT} \left(\omega_{De} - \frac{f_T}{2} \omega_{*e} \right) \right] - (2 - f_T)^2 \nu_e^2 \right\}^{1/2} \right) \tag{25}$$

In the limit of zero collision frequency, this mode reduces to an interchange mode on the trapped particles with

$$\omega^2 = \frac{\omega_{De}(\omega_{De} - f_T\omega_{*e})}{1 - f_T} \tag{26}$$

At artificially large collision frequency, $\nu_e \gg \omega_{De}, \omega_{*e}, \omega$, it becomes a complicated dissipative mode on the trapped particles with growth rate given approximately by

$$\gamma \cong \frac{2}{\nu_e(2 - f_T)}\left[\frac{4(1 - f_T)}{(2 - f_T)^2}\left(\omega_{De} - \frac{f_T}{2}\omega_{*e}\right)^2 - \omega_{De}(\omega_{De} - f_T\omega_{*e})\right] \tag{27}$$

In both limits it can be seen that ω_{De} plays an important role and can be a stabilizing influence if $|\omega_{De}| \sim |\omega_{*e}|$.

The regions of stability and instability in Eq. (25) for various values of ω_{De} and ω_{*e} can be mapped out for arbitrary ν_{eT}. It is found that the stability boundary ($\gamma = 0$) consists of two straight lines in the $\omega_{*e} - \omega_{De}$ plane (Fig. 4). Stability is obtained for

$$\frac{\omega_{De}}{\omega_{*e}} \begin{cases} \geqslant 1 \\ \leqslant -(1 - f_T) \end{cases} \tag{28}$$

We proceed now to the more general case in which the velocity space dependence of the various frequencies in Eq. (22) are included. Setting $\alpha_0 = 0$, only the integral over the trapped region of velocity space is required. As previously mentioned, the magnetic field B(s) is to be evaluated at the mirror midplane so that the trapped particle integral becomes

$$\int_{\text{trapped}} d^3r \; \frac{\omega - \omega_j^*}{\omega - \omega_{Dj} + i\nu_{j\ \text{eff}}} F_m = \frac{4}{\sqrt{\pi}} \int_0^\infty dc\; c^2 e^{-c^2}$$

$$\times \left\{ \omega - \omega_{*j} \left[1 + \eta_j \left(c^2 - \frac{3}{2} \right) \right] \right\}$$

$$\times \int_0^{\zeta_m^T} \frac{d\zeta_m}{\omega - \omega_{Dj}(c,\zeta_m) + i\nu_{j\ \text{eff}}(c)} \qquad (29)$$

where

$$\zeta_m^T = \sqrt{1 - \frac{B_{min}}{B_{max}}} = f_T$$

is the cosine of the pitch angle at the trapped-passing boundary. The integral over ζ_m can be performed analytically if the analytic fits to $\Omega(c,\zeta_m)$ as described by Eqs (5) and (6) are adopted. Using Eq. (5), we have for the trapped particles in the low beta region

$$\int_0^{\zeta_m^T} \frac{d\zeta_m}{\omega - \ell\Omega_0 c^2(\alpha_0^T - \alpha_1^T\zeta^2) + i\nu_{jT}c^{-3}}$$

$$= \frac{i}{2\sqrt{\ell\Omega_0\alpha_1^T c^2\tilde{\omega}}} \log\left(\frac{\sqrt{\tilde{\omega}} - i\sqrt{\ell\Omega_0\alpha_1^T c^2 f_T}}{\sqrt{\tilde{\omega}} + i\sqrt{\ell\Omega_0\alpha_1^T c^2 f_T}} \right) \qquad (30)$$

where

$$\tilde{\omega} = \omega - \ell\Omega_0\alpha_0^T c^2 + i\nu_{jT}c^{-3}$$

When using Eq. (30) in Eq. (29), the integral over c must, in general, be performed numerically. Also the determination of ω must be made with numerical root finding techniques. Care must be then taken in the numerical procedures to remain on the correct branch of the complex logarithm and square root.

Figures 5-8 show growth rate γ obtained from the dispersion relation Eq. (22) versus ω_{*e} for various plasma situations. In each of the figures, growth rate γ, Spitzer electron collision frequency ν_e, and diamagnetic frequency ω_* are in units of $\ell\Omega$. The calculations are representative of the interior, low beta region of EBT in that Ω' — reflected in α_0^T, α_1^T of Eq. (30) — was obtained from Eq. (5) and f_T was taken as 0.7.

Figure 5 shows growth rates for various values of $\nu_e/\ell\Omega_0$ with $T_e/T_i = 1$ and $\eta_e = \eta_i = 0$. The instability does have much the character of a dissipative mode since the growth rate and the range of ω_* over which the mode is unstable increases as ν_e decreases. The crucial point is for small enough $\omega_*/\ell\Omega_0$ the mode is indeed stabilized as indicated by the simplified dispersion relation shown in Eq. (24). The dashed line in Fig. 5 is the growth rate obtained from Eq. (24) for the case $\nu_e/\omega_{De} = 1.0$. If the velocity dependence of the $\omega_{Dj}(c,\zeta_m)$ and $\nu_{j\ eff}(c)$ in Eq. (22) is artificially reduced, the $\nu_e/\ell\Omega_0 = 1.0$ curve in Fig. 5 continuously approaches the dashed curve. This verifies the validity of the numerical procedure in the limit of velocity independent drift and collision frequencies.

Figure 6 shows the effect of including a temperature gradient, η, for the case $\nu_e/\ell\Omega_0 = 1.0$, $T_e/T_i = 1.0$. A normal temperature gradient,

$\eta_e = \eta_i = 1.0$, increases the growth rates in the unstable region but apparently has little effect on the marginal stability point. A reversed temperature gradient, $\eta_e = \eta_i = -1.0$, pushes the marginal point to higher ω_* and also reduces growth rates. Figure 7 shows growth rates for various values of T_e/T_i for the case $\nu_e/\ell\Omega_0 = 0.1$, $\eta_e = \eta_i = 0$. Increasing T_e/T_i is clearly a stabilizing effect.

Equation (28) indicates instability for reversed density gradients when $\omega_{*e} \lesssim -\omega_{De}/(1 - f_T)$. In the present instance, $f_T = 0.3$; the instability should exist for $\omega_{*e}/\ell\Omega_0 \lesssim -3.3$. Figure 8 shows growth rates for negative values of ω_{*e} with $T_e/T_i = 1$, $\eta_e = \eta_i = 0$, and $\nu_e/\ell\Omega_0$ ranging from 0.2 to 1.0. Obviously, the marginal points extend to much larger $|\omega_*/\ell\Omega_0|$ than is the case for normal gradients. Also in contrast to the normal gradients, the growth rate decreases with decreasing collisionality. Calculations have also been performed using the fit given in Eq. (6) for Ω' in the high beta, reversed ∇B region near the outer portion of the annulus. Here the pressure gradients are normal, $\omega_{*e} > 0$, but the magnetic drift frequency ω_{De} is negative and large, $\langle\Omega'\rangle \cong 2.95$. The instability essentially disappears under these conditions since we were unable to find any unstable roots for $|\omega_{*e}/\ell\Omega_0| < 20$ at any collisionality $\nu_e/\ell\Omega_0 < 5$.

4. PURE FLUTE MODES

Next will be considered the case in which the potential is assumed not to vary along a magnetic field line, $\alpha_0 = 1$, $\alpha_n = 0$, $n \neq 0$. As is clear from Eq. (22), the passing particles now make a contribution to

the nonadiabatic response. As in the previous section, we first examine the simplified dispersion relation obtained by replacing integrals over the velocity dependent frequencies ω_{Dj}, ω_j^*, $\nu_{j\ eff}$ by constant values. The dispersion relation then has the form

$$\frac{1}{T_e} + \frac{1}{T_i} = \frac{1}{T_e}\left[(1 - f_T)\frac{\omega - \omega_{*e}}{\omega - \omega_{DeP} + i\nu_{eP}} + f_T \frac{\omega - \omega_{*e}}{\omega - \omega_{DeT} + i\nu_{eT}}\right]$$

$$+ \frac{1}{T_i}\left[(1 - f_T)\frac{\omega - \omega_{*i}}{\omega - \omega_{DiP} + i\nu_{iP}} + f_T \frac{\omega - \omega_{*i}}{\omega - \omega_{DiT} + i\nu_{iT}}\right] \quad (31)$$

where j = e,i refers to particle species and T,P refers to trapped or passing. This equation is cubic in ω and contains six independent parameters.

Considering the relative small size of $\langle\Omega'\rangle_{passing}$, the enhancement of ν_{jP} [Eq. (10)] and the estimates of $\langle\Omega\rangle$ and ν_j given in Table II, it can be seen that except for large mode numbers, ℓ, the following ordering holds

$$\omega_{DjP} < \nu_{jP}\ ,\ \omega_j^*$$

Also in general

$$\nu_{jT} < \omega_{DjT}\ ,\ \omega_j^*$$

We therefore consider the limit $\omega_{DjP} \to 0$, $\nu_{jT} \to 0$. For convenience it is also assumed that $T_e = T_i$ so that $\omega_{*e} = -\omega_{*i}$ and $\omega_{De} = -\omega_{Di}$. Equation (31) then reduces to

$$2 = \left[(1 - f_T)\frac{\omega - \omega_{*e}}{\omega + i\nu_{eP}} + f_T\frac{\omega - \omega_{*e}}{\omega - \omega_{De}}\right] + \left[(1 - f_T)\frac{\omega + \omega_{*e}}{\omega + i\nu_{iP}} + f_T\frac{\omega + \omega_{*e}}{\omega + \omega_{De}}\right] \tag{32}$$

The resulting dispersion relation is of the form

$$i(1 - f_T)\left(\frac{\nu_e + \nu_i}{2}\right)\omega^3 - \left\{f_T\omega_{De}(\omega_{De} - \omega_{*e}) + (1 - f_T)\left|\nu_e\nu_i - \frac{1}{2}\omega_{*e}(\nu_e \quad \nu_i)\right|\right\}\omega^2$$

$$-i(\nu_e + \nu_i)\omega_{De}\left[\frac{1}{2}(1 + f_T)\omega_{De} - f_T\omega_{*e}\right]\omega$$

$$+ \omega_{De}\left[\nu_e\nu_i(\omega_{De} - f_T\omega_{*e}) - \frac{1}{2}(1 - f_T)\omega_{*e}\omega_{De}(\nu_e - \nu_i)\right] = 0 \tag{33}$$

For small collision frequencies, an approximate solution to Eq. (33) can be obtained by balancing the cubic and quadratic terms

$$\omega = -i\frac{2f_T}{(1 - f_T)}\frac{\omega_{De}(\omega_{De} - \omega_{*e})}{\nu_{eP} + \nu_{iP}} \tag{34}$$

or since $\nu_{jP} = \nu_j/(1 \quad f_T)^?$

$$\gamma = 2f_T(1 - f_T)\frac{\omega_{De}(\omega_{*e} - \omega_{De})}{\nu_e + \nu_i} \tag{35}$$

This growth rate is very similar to the simplest form of the dissipative trapped-ion mode in tokamaks. For the present mode however, it is the collisions of the passing particles which are destabilizing.

This instability might justifiably be called a dissipative passing-particle mode. An important feature of Eq. (35) is the presence of the ω_D term, which is stabilizing if ω_{*e}/ω_{De} is sufficiently small. The stability boundaries are similar to those of the mode discussed in the previous section.

$$\frac{\omega_{De}}{\omega_{*e}} \begin{cases} \geqslant 1 \\ \leqslant 0 \end{cases} \tag{36}$$

Note that even though the mode has a dissipative character, the conditions for marginal stability are very similar to the requirements of MHD stability.

We return now to Eq. (22) and include the velocity dependence of ω_{Tj}^*, ω_{Dj}, and ν_j. The velocity space integral over passing particles has the same form as Eq. (29), except that the range of integration is $\zeta_m^T \leqslant \zeta_m \leqslant 1$. Making use of the representation for Ω' in Eq. (5), we have for the passing particles in the low beta region,

$$\int_{\zeta_m^T}^{1} \frac{d\zeta_m}{\omega - \ell\Omega_0 c^2[\alpha_0^P - \alpha_1^P(1 - \zeta_m)^2] + i\nu_{jP}c^{-3}} = \frac{1}{\sqrt{q}} \ell n \left[\frac{\sqrt{q} - 2a(1 - \zeta_m^T)}{\sqrt{q} + 2a(1 - \zeta_m^T)}\right]$$

where

$$a = \ell\Omega_0\alpha_1^P c^2$$

$$q = 4a(a - \tilde{\omega})$$

$$\tilde{\omega} = \omega - \ell\Omega_0(\alpha_0^P - \alpha_1^P)c^2 + i\nu_{jP}c^{-3}$$

Again the integral over c and the determination of the roots of the dispersion relation must be carried out numerically.

Figure 9 shows the growth rate γ obtained from Eq. (22) with $\alpha_0 = \delta_{n0}$ for various electron-ion temperature ratios. The growth rates are noticeably higher, and the marginal values of ω_{*e} are lower than the analogous results with no nonadiabatic passing particle response (Fig. 7). This enhancement of the instability might well be expected since the inclusion of passing particles serves to increase the number of particles having $\omega_D < \omega_*$. The marginal point for $T_e/T_i = 1$ extends below $\omega_{*e}/\ell\Omega_0 = 1$ in contrast to the results obtained from the simplified dispersion relation [Eq. (36)]. However, the mode is still stabilized at a nonnegligible value of ω_{*e} ($\omega_{*e}/\ell\Omega_0 < 0.6$, in this case). Calculations have been done for nonzero η_e, η_i, and for various values of $\nu/\ell\Omega_0$, but the trends are essentially the same as shown in Figs 5 and 6 for the mode with purely adiabatic passing particles. The simplified dispersion relation is cubic and complex; therefore it is capable of more than one unstable root. However, searches in the complex ω plane have not yielded any additional unstable roots for Eq. (22).

5. CONCLUSIONS

Employing a simple bounce-averaged drift kinetic model, we have investigated the electrostatic stability properties of low frequency drift waves in the frequency ordering appropriate for the EBT device. Care has been taken to model (at least in an elementary way) the features which distinguish the physics of EBT from those of tokamaks; i.e., the

large magnitude and velocity space dependence of the magnetic precessional frequency Ω, the relatively small collisionality ν_j/Ω_j, the enhancement of the effective collision frequency for passing-particles, and the closed nature of the field lines. The equations for the structure of modes along field lines have not as yet been solved. Instead the consequences of two assumptions were investigated. First, it was assumed that the variation of the potential had much larger scale length than the length of a single sector, and that the average of the potential around the torus vanished. In this case, the passing particles respond completely adiabatically to the drift wave. Second, the case of pure flute modes was investigated. Here the passing particles also had a nonadiabatic response. In each case, we found for normal gradients ($\omega_*/\Omega > 0$) instability was possible for sufficiently large $\omega_*/\ell\Omega$. The modes had a dissipative character in that the growth rates and the region of possible instability in $\omega_* - \Omega$ space increased with decreasing collisionality. It was also found that the magnitude and velocity space dispersion of Ω are significant stabilizing influences, since in most cases the modes are completely stabilized for $\omega_*/\ell\Omega \lesssim 1$. For the case of reversed gradients ($\omega_*/\Omega < 0$), stability is greatly enhanced and growth rates decrease with decreasing ν/Ω.

Much additional analysis of the linear and nonlinear behavior will be necessary in order to assess whether these modes are of any real importance in scaling the EBT concept to a reactor device. The results of the present study must be considered to be encouraging in that the modes can be stabilized by proper tailoring of the ω_* and Ω profiles.

Also the necessary profiles appear to be consistent with the requirements of MHD stability and neoclassical transport. To see this specifically, suppose that equilibrium profiles of the type shown in Figs 1a and 1b were those actually obtained in experiment. In the interior region where the pressure profile is very flat, modes described by Eq. (36), for example, would be stabilized by virtue of $\omega_* < \omega_D$. Near the outer region of the annulus, we have $\omega_*\omega_D < 0$, which the present analysis shows to be positively stable. The only region in which there would appear danger of instability is in a narrow zone where ∇B changes sign (see Fig. 4). Whether such stable equilibrium can actually be maintained by the tailoring of heating and fueling profiles can only be determined by transport modeling and experimentation.

The model used here is quite crude in many respects, and a number of improvements are being incorporated; others need to be. The weakness of the bounce averaging procedure for the ions is a serious concern. We are now in the process of carrying out a full drift-kinetic analysis, which will also permit the inclusion of Landau damping effects. A strong stabilizing influence was found to be the velocity space dispersion of the precessional drift frequency. Because in toroidal geometry, the inward shift of a particle drift surface (essentially the neoclassical step size) is velocity-space dependent, particles also become radially decorrelated on the drift time scale, Ω^{-1}. This toroidal effect adds to the dispersion in the particle orbits and probably limits the scale length for radial variations in the potential. The radial particle drifts and the strong radial shear in Ω point up the need for

an investigation of the radial eigenvalue problem. It would also be desirable to study the effects of more realistic collision operators than the simple Krook model used here.

ACKNOWLEDGEMENTS

The authors would like to express their appreciation to B. V. Waddell, who has been very generous with his time and experience in trapped particle mode theory. Also to J. D. Callen, K. T. Tsang, D. A. Spong, E. F. Jaeger, L. W. Owen, and R. C. Goldfinger for a number of very helpful discussions. Other helpful discussions were shared with J. B. McBride and N. A. Krall of Science Applications, Inc.

Table I. EBT device parameters

	EBT-I	EBTR
Density, cm^{-3}	3×10^{12}	1.5×10^{14}
T_i	100 eV	15 keV
T_e	300 eV	15 keV
B on axis	6 kG	25 kG
Plasma radius, a	10 cm	100 cm
Toroidal radius, R_T	100 cm	60 cm
Number of sectors, N	24	48
Typical magnetic radius of curvature, R_c	18.8 cm	2.7 m

Table II. EBT device frequency orderings

	EBT-I	EBTR
$\lvert\omega_{*min}\rvert = \frac{2T_e}{m_e\omega_{ce}a^2}$	1.0×10^5/sec	1.2×10^4/sec
$\lvert\omega_{*max}\rvert = 2\frac{a}{\rho_i}\frac{T_e}{m_e\omega_{ce}a^2}$	5.9×10^6/sec	1.7×10^6/sec
$\langle\Omega_e\rangle$ low beta region	-1.03×10^5/sec	-1.4×10^3/sec
$\langle\Omega_e\rangle$ high beta region	4.2×10^5/sec	5.7×10^3/sec
$\omega_{be} = \frac{v_e}{L_s}$	2.8×10^7/sec	6.5×10^6/sec
$\omega_{bi} = \frac{v_i}{L_s}$	3.7×10^5/sec	1.1×10^5/sec
$\omega_{Te} = \frac{v_e}{R_T}$	7.3×10^6/sec	8.6×10^5/sec
$\omega_{Ti} = \frac{v_i}{R_T}$	9.8×10^4/sec	1.4×10^4/sec
ν_e	3×10^4/sec	3.5×10^3/sec
ν_i	3.6×10^3/sec	5×10^1/sec

REFERENCES

[1] KADOMTSEV, B.B., POGUTSE, O.P., Zh. Eksp. Teor. Fiz. [Sov. Phys. — JETP] 24 (1967) 1172.

[2] KADOMTSEV, B.B., POGUTSE, O.P., Nucl. Fusion 11 (1971) 67.

[3] DANDL, R.A., DORY, R.A., EASON, H.O., GUEST, G.E., ORNL/TM-4941, Oak Ridge, Tennessee (June 1975).

[4] McALEES, D.G., UCKAN, N.A., BETTIS, E.S., HEDRICK, C.L., ORNL/TM-5669, Oak Ridge, Tennessee (November 1976).

[5] JAEGER, E.F., SPONG, D.A., HEDRICK, C.L., Phys. Rev. Lett. 40 (1978) 866.

[6] COLESTOCK, P.L., CONNER, K.A., DANDL, R.A., Bull. Am. Phys. Soc. 22 (1977) 1146, to be published in Phys. Rev. Lett.

[7] MOROZOV, A.I., SOLOVEV, L.S., *Reviews of Plasma Physics*, Vol. 1, p. 290, Consultants Bureau (LEONTOVICH, M.A., Ed.), New York, 1969.

[8] NELSON, D.B., HEDRICK, C.L., ORNL/TM-5967, Oak Ridge, Tennessee (December 1977), to be published in Nucl. Fusion.

[9] SPONG, D.A., HARRIS, E.G., HEDRICK, C.L., ORNL/TM-6215, Oak Ridge, Tennessee (1978).

[10] ROSENBLUTH, M.N., ROSS, D.W., KOSTOMAROV, D.P., Nucl. Fusion 12 (1972) 3.

LIST OF CAPTIONS

Fig. 1. Expected equilibrium profiles in EBT (a) magnetic field at the midplane B/B_0, density of the toroidal core n/n_0, and density of the annulus (b) poloidal drift frequency Ω and diamagnetic drift frequency ω_* for profiles in (a).

Fig. 2. Ω'/c^2 versus $\zeta_m = \nu_{\| m}/\nu$ for points in the low beta region and the high beta region.

Fig. 3. Bumpy cylinder geometry.

Fig. 4. Stability regions versus ω_D and ω_* for velocity independent ω_D, ω_*, ν_e. The passing particles were assumed to respond adiabatically.

Fig. 5. Growth rate versus $\omega_{*e}/\ell\Omega_0$ for various values of $\nu_e/\ell\Omega_0$.

Fig. 6. Growth rate versus $\omega_{*e}/\ell\Omega_0$ for various values of $\eta_e = \eta_i$.

Fig. 7. Growth rate versus $\omega_{*e}/\ell\Omega_0$ for various values of T_e/T_i.

Fig. 8. Growth rate for negative values of $\omega_{*e}/\ell\Omega_0$.

Fig. 9. Growth rate of pure flute modes versus $\omega_{*e}/\ell\Omega_0$ for various values of T_e/T_i.

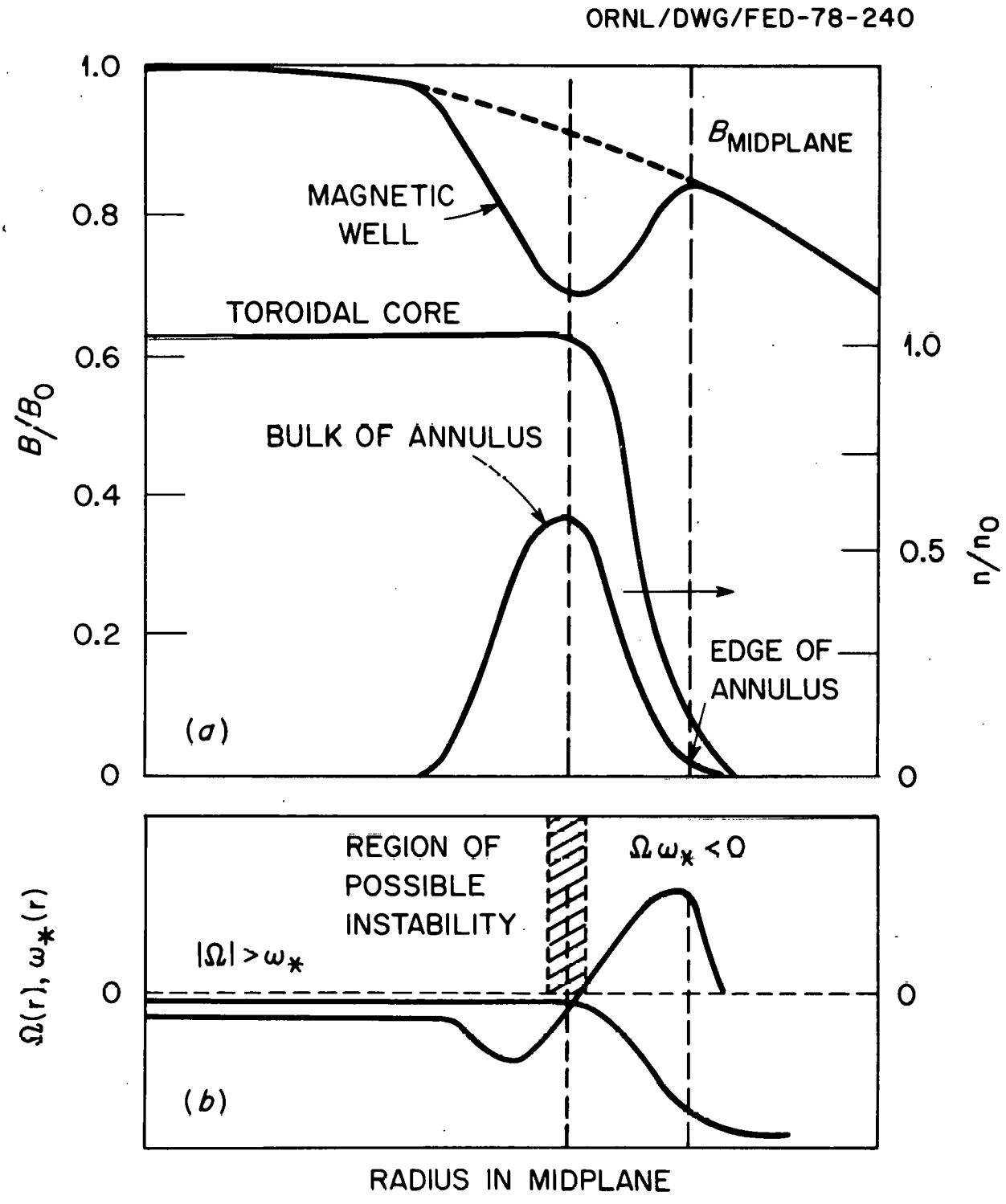
ORNL/DWG/FED-78-240
1.0
0.8
0.6
0.4
0.2
0
B/B_0
$B_{MIDPLANE}$
MAGNETIC WELL
TOROIDAL CORE
BULK OF ANNULUS
EDGE OF ANNULUS
(a)
1.0
0.5
0
n/n_0
REGION OF POSSIBLE INSTABILITY
$\Omega\omega_* < 0$
$|\Omega| > \omega_*$
$\Omega(r), \omega_*(r)$
0
(b)
RADIUS IN MIDPLANE

Fig. 1.

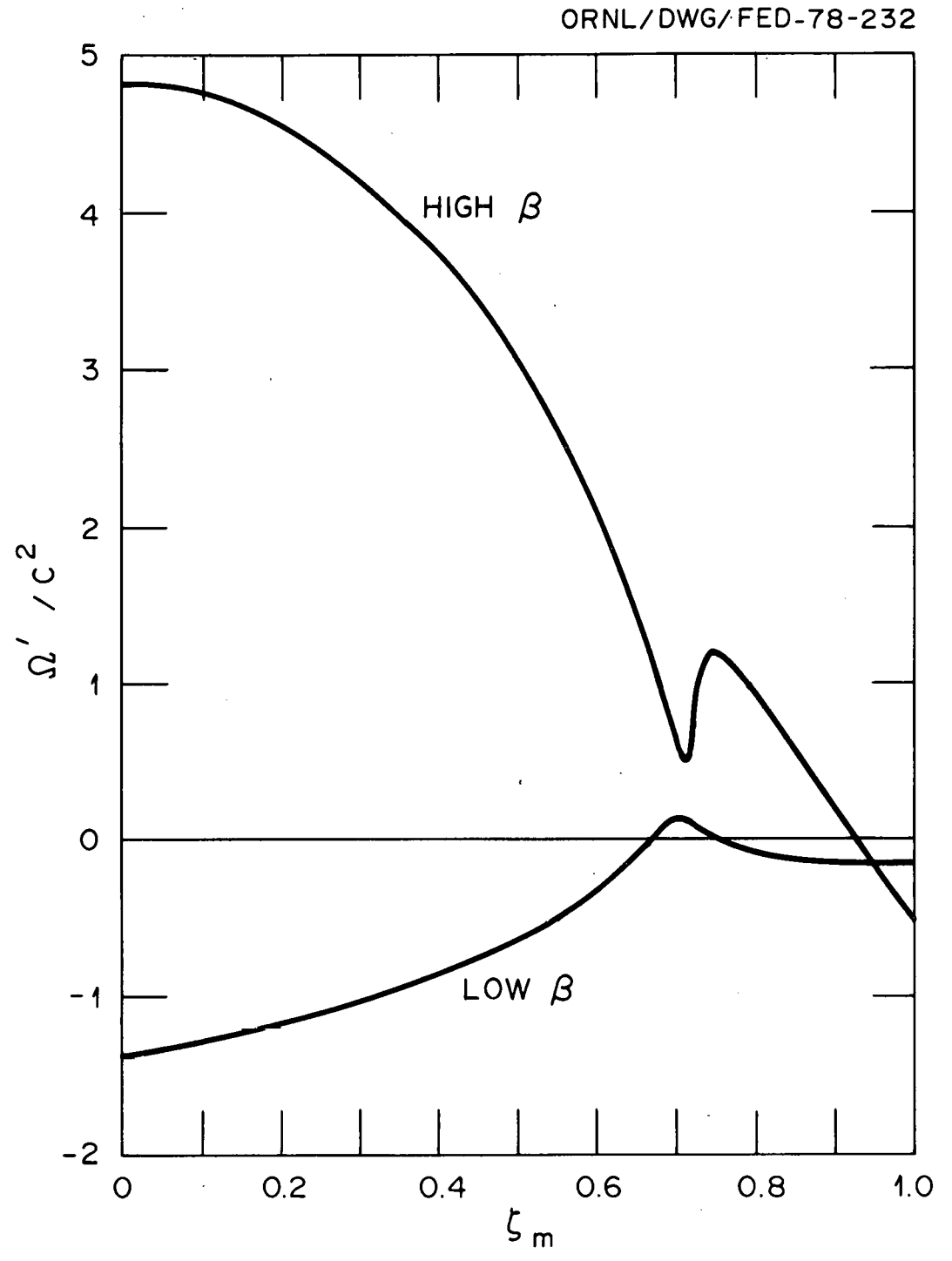

Fig. 2.

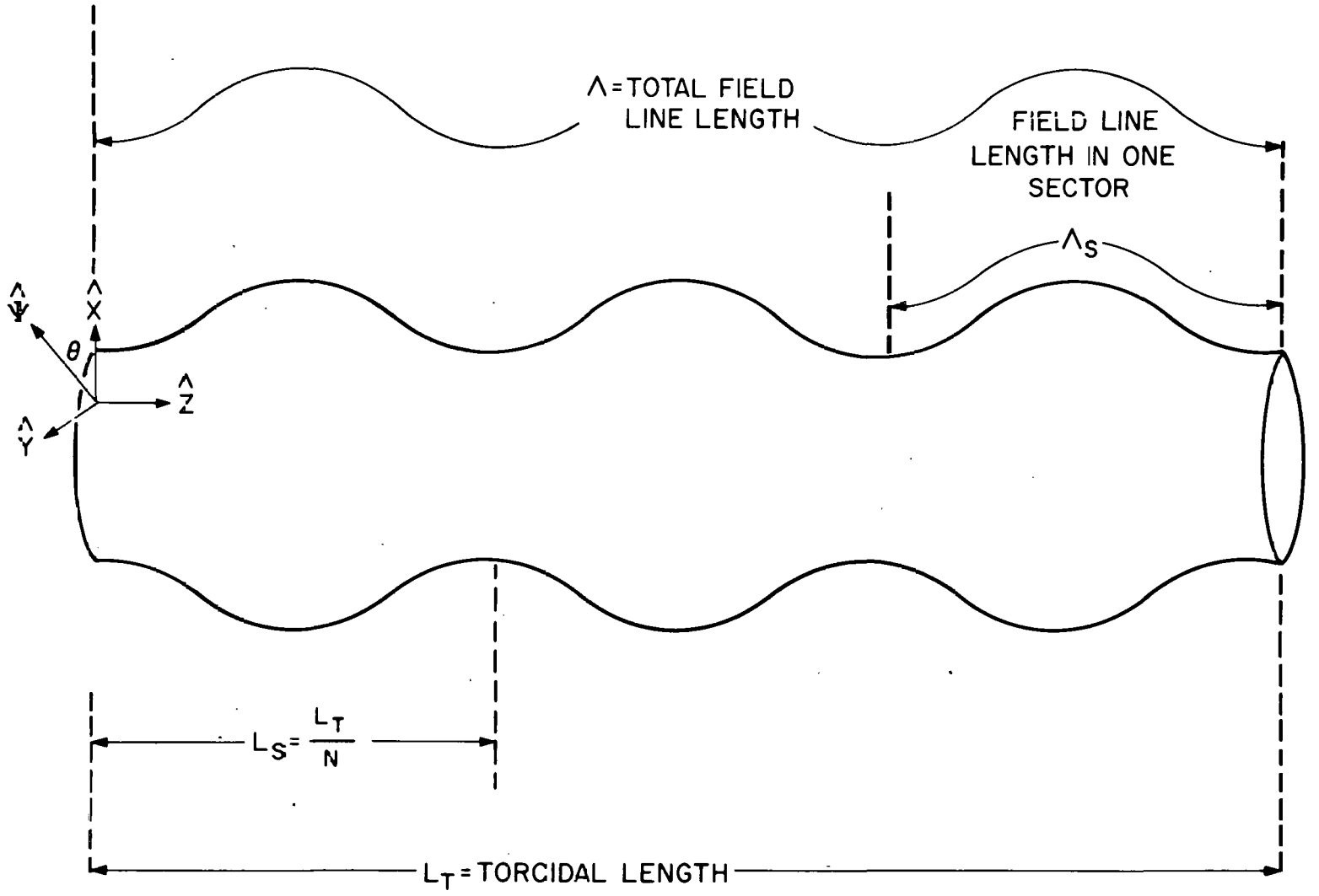
Λ=TOTAL FIELD LINE LENGTH
FIELD LINE LENGTH IN ONE SECTOR
Λs
θ
Ψ̂
X̂
Ẑ
Ŷ
Ls= LT/N
LT=TORCIDAL LENGTH

Fig. 3.

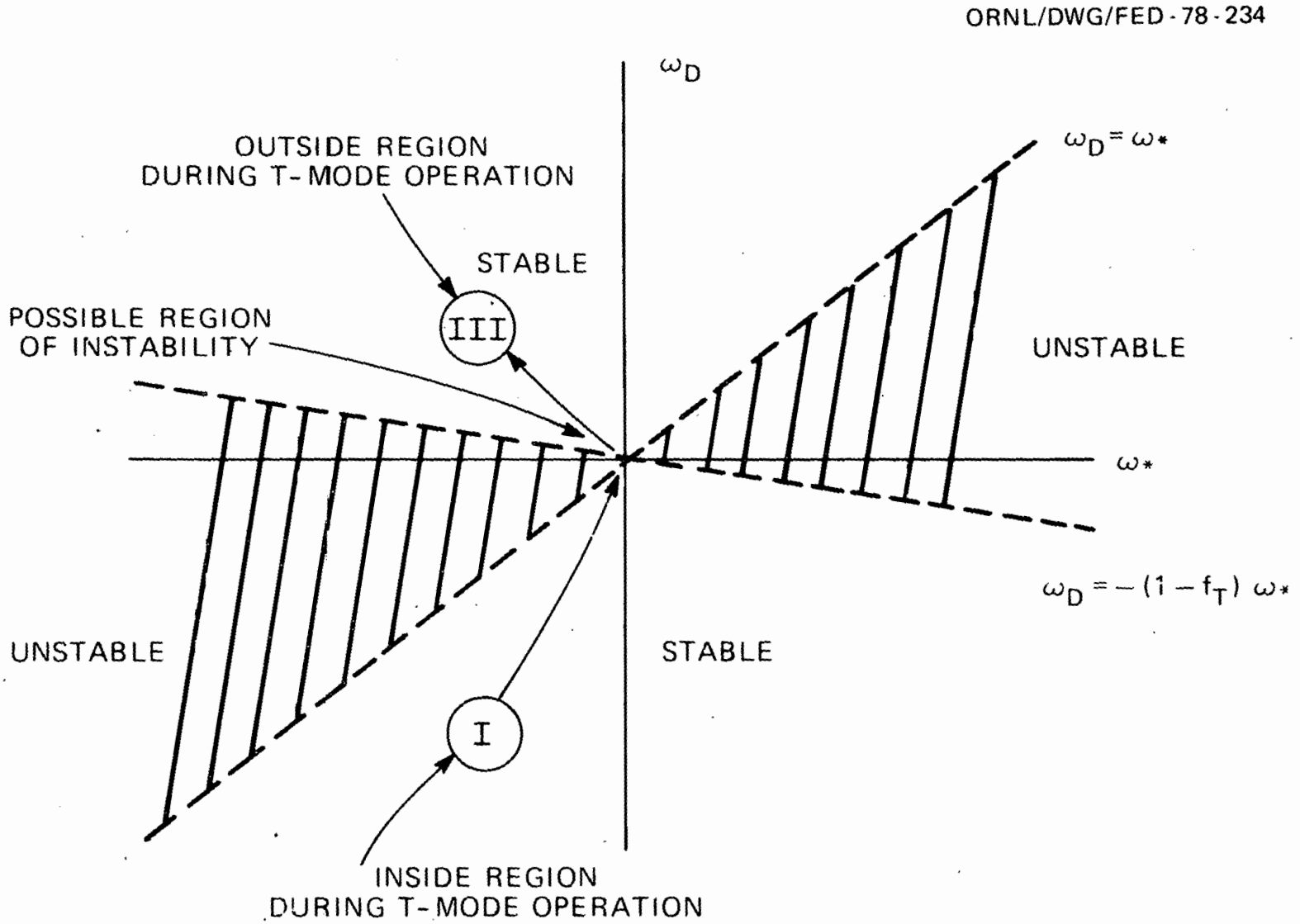
ORNL/DWG/FED-78-234
ω_D
OUTSIDE REGION
DURING T-MODE OPERATION
STABLE
POSSIBLE REGION
OF INSTABILITY
III
$\omega_D = \omega_*$
UNSTABLE
ω_*
$\omega_D = -(1 - f_T)\ \omega_*$
UNSTABLE
STABLE
I
INSIDE REGION
DURING T-MODE OPERATION

Fig. 4.

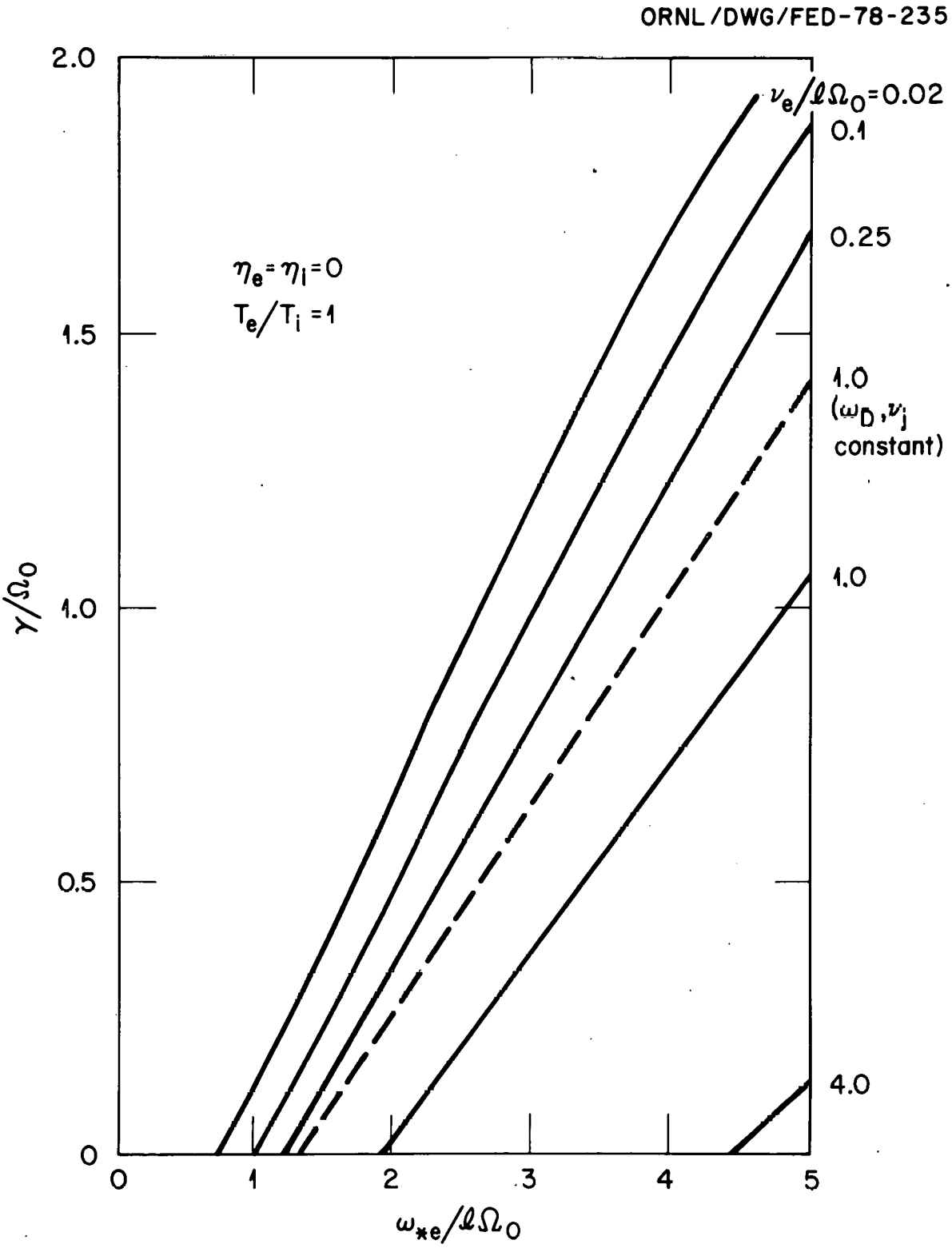
ORNL/DWG/FED-78-235
2.0
1.5
1.0
0.5
0
0
1
2
3
4
5
γ/Ω_0
$\omega_{*e}/\ell\Omega_0$
$\eta_e = \eta_i = 0$
$T_e/T_i = 1$
$\nu_e/\ell\Omega_0 = 0.02$
0.1
0.25
1.0
(ω_D, ν_j constant)
1.0
4.0

Fig. 5.

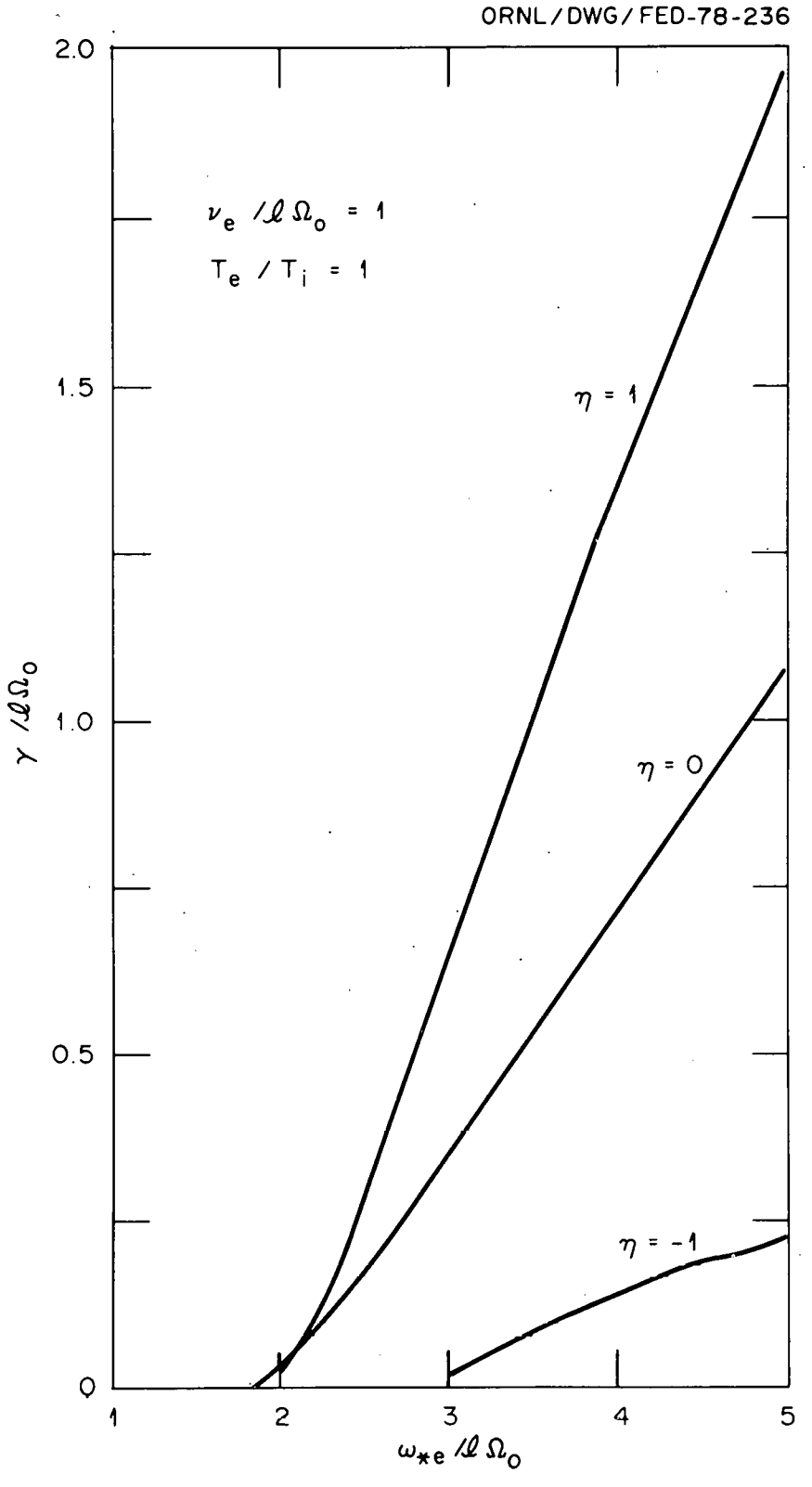
ORNL/DWG/FED-78-236
2.0
1.5
1.0
0.5
0
1
2
3
4
5
$\nu_e / \ell \Omega_o = 1$
$T_e / T_i = 1$
$\eta = 1$
$\eta = 0$
$\eta = -1$
$\gamma / \ell \Omega_o$
$\omega_{*e} / \ell \Omega_o$

Fig. 6.

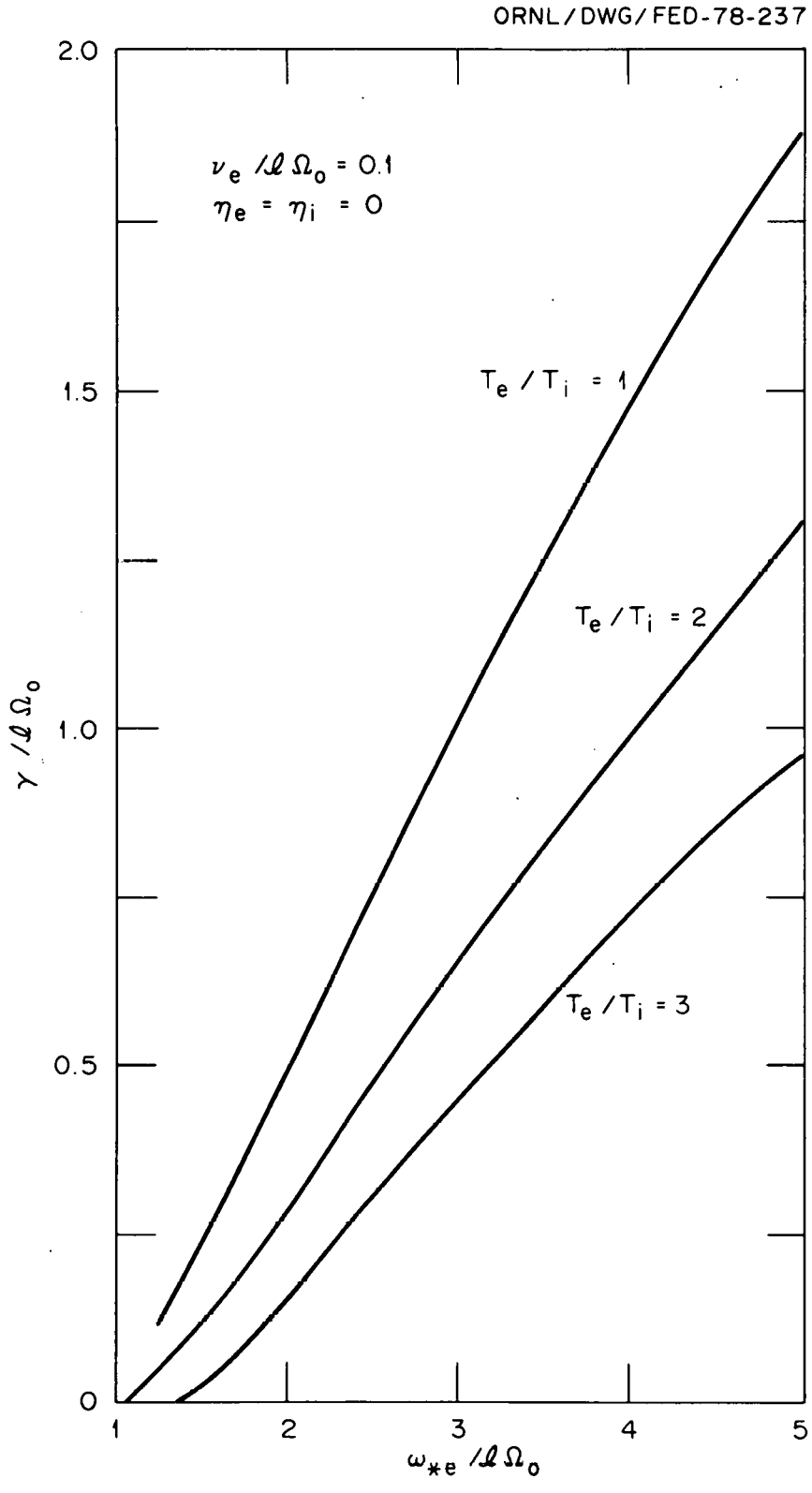
ORNL/DWG/FED-78-237
2.0
1.5
1.0
0.5
0
1
2
3
4
5
$\nu_e / \ell \Omega_o = 0.1$
$\eta_e = \eta_i = 0$
$T_e / T_i = 1$
$T_e / T_i = 2$
$T_e / T_i = 3$
$\gamma / \ell \Omega_o$
$\omega_{*e} / \ell \Omega_o$

Fig. 7.

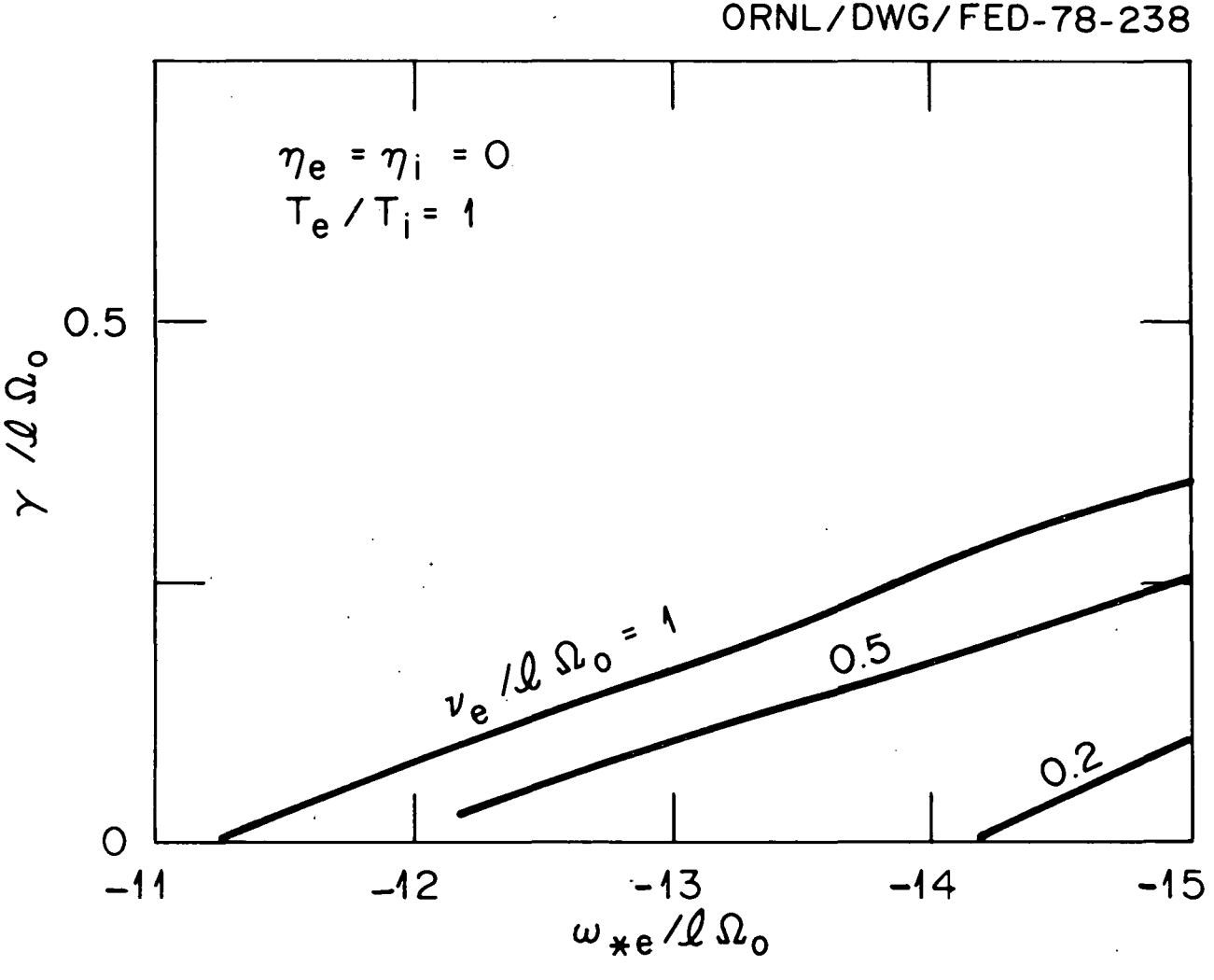
ORNL/DWG/FED-78-238
$\eta_e = \eta_i = 0$
$T_e / T_i = 1$
$\gamma / \ell \Omega_0$
0.5
0
$\nu_e / \ell \Omega_0 = 1$
0.5
0.2
-11
-12
-13
-14
-15
$\omega_{*e} / \ell \Omega_0$

Fig. 8.

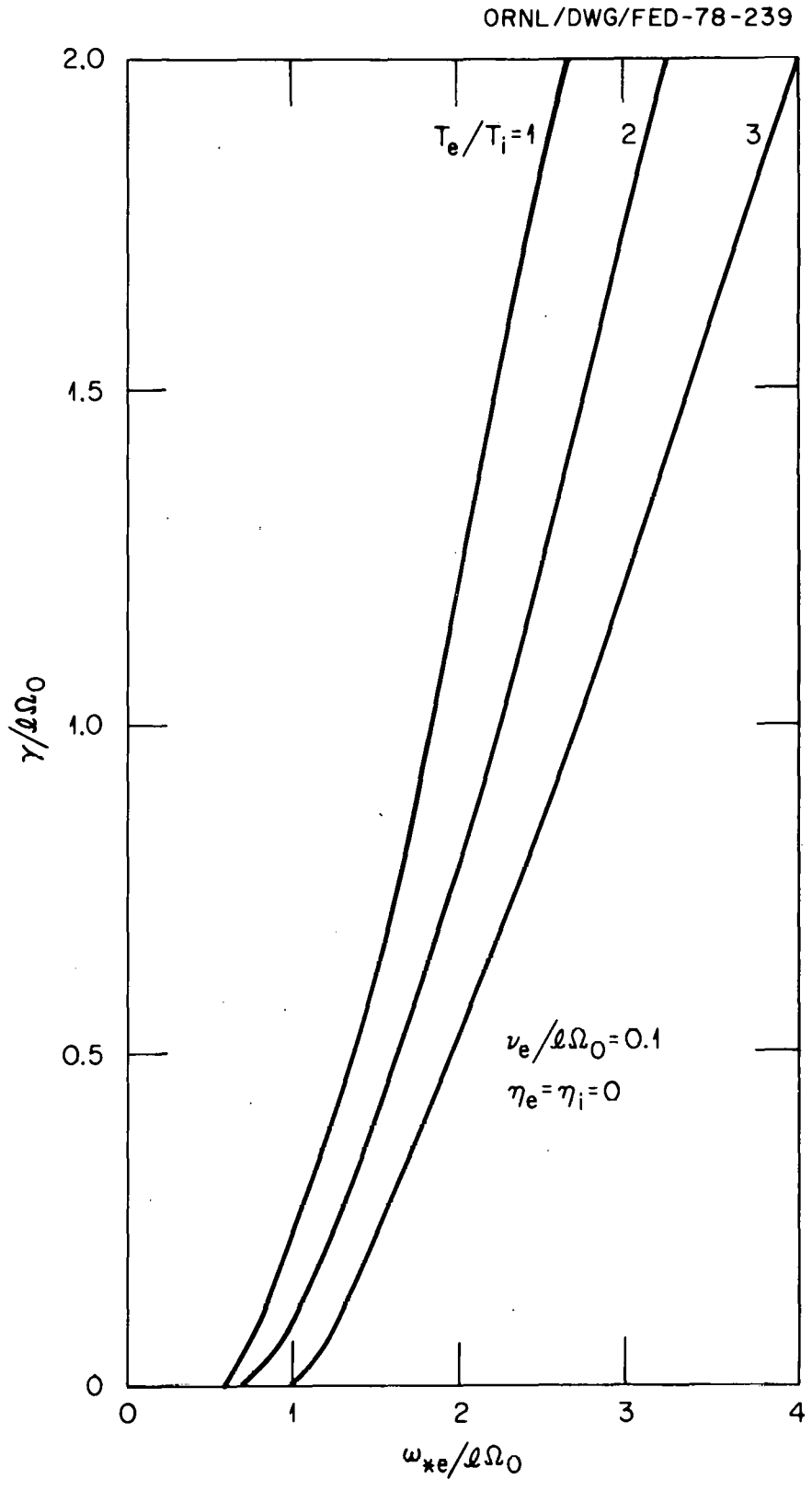
ORNL/DWG/FED-78-239
2.0
1.5
1.0
0.5
0
$\gamma/\ell\Omega_0$
$T_e/T_i=1$
2
3
$\nu_e/\ell\Omega_0=0.1$
$\eta_e=\eta_i=0$
0
1
2
3
4
$\omega_{*e}/\ell\Omega_0$

Fig. 9.

ORNL/TM-6318
Dist. Category UC-20g

INTERNAL DISTRIBUTION

1. L. A. Berry
2. J. D. Callen
3. R. A. Dandl
4. R. A. Dory
5. G. G. Kelley
6. H. H. Haselton
7. P. N. Haubenreich
8. M. S. Lubell
9. O. B. Morgan
10. H. Postma
11. M. W. Rosenthal
12. J. Sheffield
13. D. Steiner
14-46. D. B. Batchelor
47. C. L. Hedrick
48-49. Laboratory Records Department
50. Laboratory Records, ORNL-RC
51. Document Reference Section
52-53. Central Research Library
54. Fusion Energy Division Library
55. Fusion Energy Division Communications Center
56. ORNL Patent Office

EXTERNAL DISTRIBUTION

57. Bibliothek, Max-Planck Institute für Plasmaphysik, 8046 Garching bei München, Federal Republic of Germany
58. Bibliothèque, Service du Confinement des Plasmas, C.E.A., B.P. No. 6, 92, Fontenay-aux Roses (Seine), France
59. Lung Cheung, Department of Electronics, University Science Center, The Chinese University of Hong Kong, Shatin, N.T., Hong Kong
60. J. F. Clarke, Office of Fusion Energy, G-234, Department of Energy, Washington, DC 20545
61. R. W. Conn, Fusion Technology Program, Nuclear Engineering Department, University of Wisconsin, Madison, WI 53706
62. CTR Library, c/o Alan F. Haught, United Technologies Research Laboratory, East Hartford, CT 06108
63. CTR Reading Room, c/o Allan N. Kaufman, Physics Department, University of California, Berkeley, CA 94720
64. J. Narl Davidson, School of Nuclear Engineering, Georgia Institute of Technology, Atlanta, GA 30332
65. Documentation S.I.G.N., Département de la Physique du Plasma et de la Fusion Controlée, Association EURATOM-CEA sur la Fusion, Centre d'Études Nucléaires, B.P. 85, Centre du TRI, 38041 Grenoble, Cedex, France
66. W. R. Ellis, Office of Fusion Energy, G-234, Department of Energy, Washington, DC 20545
67. Harold K. Forsen, Exxon Nuclear Co., Inc., 777 106th Avenue, N.E., C-000777, Bellevue, WA 98009
68. Harold P. Furth, Princeton Plasma Physics Laboratory, Princeton University, Forrestal Campus, P.O. Box 451, Princeton, NJ 08540
69. Roy W. Gould, California Institute of Technology, Mail Stop 116-81, Pasadena, CA 91125
70. Robert L. Hirsch, Exxon Research and Engineering, P.O. Box 101, Florham Park, NJ 07932

71. Raymond A. Huse, Manager, Research and Development, Public Service Gas and Electric Company, 80 Park Place, Newark, NJ 07101
72. T. Hsu, Office of Fusion Energy, G-234, Department of Energy, Washington, DC 20545
73. V. E. Ivanov, Physical-Technical Institute of the Ukranian Academy of Sciences, Sukhumi, U.S.S.R.
74. A. Kadish, Office of Fusion Energy, G-234, Department of Energy, Washington, DC 20545
75. L. M. Kovrizhnikh, Lebedev Institute of Physics, Academy of Sciences of the U.S.S.R., Leninsky Prospect 53, Moscow, U.S.S.R.
76. Guy Laval, Groupe de Physique Théorique, Ecole Polytechnique, 91 Palaiseau, Paris, France
77. Library, Centre de Recherches en Physique des Plasma, 21 Avenue des Bains, 1007, Lausanne, Switzerland
78. Library, Culham Laboratory, United Kingdom Atomic Energy Authority, Abingdon, Oxon, OX14 3DB, United Kingdom
79. Library, FOM-Institut voor Plasma — Fysica, Rijnhuizen, Jutphaas, Netherlands
80. Library, Institute for Plasma Physics, Nagoya University, Nagoya, Japan 464
81. Library, International Centre for Theoretical Physics, Trieste, Italy
82. Library, Laboratorio Gas Ionizzati, Frascati, Italy
83. Dsumber G. Lominadze, Academy of Sciences of the Georgian S.S.R., 8 Dzerzhinski St., 38004, Tbilisi, U.S.S.R.
84. Oscar P. Manley, Office of Fusion Energy, G-234, Department of Energy, Washington, DC 20545
85. D. G. McAlees, Exxon Nuclear Co., Inc., Research and Technology Laser Enrichment Department, 2955 George Washington Way, Richland, WA 99352
86. J. E. McCune, School of Engineering, Department of Aeronautics and Astronautics, Bldg. 37-391, Massachusetts Institute of Technology, Cambridge, MA 02139
87. Claude Mercier, Service du Theorie des Plasmas, Centre d'Études Nucléaires, Fontenay-aux-Roses (Seine), France
88. K. G. Moses, Office of Fusion Energy, G-234, Department of Energy, Washington, DC 20545
89. D. Pfirsch, Institute for Plasma Physics, 8046 Garching bei München, Federal Republic of Germany
90. Plasma Physics Group, Department of Engineering Physics, Australian National University, P.O. Box 4, Canberra A.C.T. 2600, Australia
91. Robert E. Price, Office of Fusion Energy, G-234, Department of Energy, Washington, DC 20545
92. A. Rogister, Institute for Plasma Physics, KFA, Postfach 1913, D-5170, Jülich 1, Federal Republic of Germany
93. W. Sadowski, Office of Fusion Energy, G-234, Department of Energy, Washington, DC 20545
94. V. D. Shafranov, I. V. Kurchatov Institute of Atomic Energy, 46 Ulitsa Kurchatova, P.O. Box 3402, Moscow, U.S.S.R.

95. Yu. S. Sigov, Institute of Applied Mathematics of the U.S.S.R. Academy of Sciences, Miuskaya, Sq. 4, Moscow A-47, U.S.S.R.
96. W. M. Stacey, Jr., School of Nuclear Engineering, Georgia Institute of Technology, Atlanta, GA 30332
97. J. B. Taylor, Culham Laboratory, United Kingdom Atomic Energy Authority, Abingdon, Oxon, OX14 3DB, United Kingdom
98. Thermonuclear Library, Japan Atomic Energy Research Institute, Tokai, Naka, Ibaraki, Japan
99. Francisco Verdaguer, Director, Division of Fusion, Junta de Energia Nuclear, Madrid 3, Spain
100. Director, Research and Technical Support Division, Department of Energy, Oak Ridge Operations, P.O. Box E, Oak Ridge, TN 37830
101-276. Given distribution as shown in TID-4500, Magnetic Fusion Energy (Distribution Category UC-20g, Theoretical Plasma Physics)